JOURNAL OF MATERIALS SCIENCE 35 (2000) 249–257

Hydration of alkali-activated ground granulated blast furnace slag

S. SONG*, D. SOHN*, H. M. JENNINGS*‡, T. O. MASON*
*Department of *Materials Science and Engineering and ‡Civil Engineering, Northwestern University, Evanston, IL 60208*
E-mail: h-jennings@nwu.edu

The hydration of ground granulated blast furnace slag (GGBFS) at 25 °C in controlled pH environments was investigated during 28 days of hydration. GGBFS was activated by NaOH, and it was found that the rate of reaction depends on the pH of the starting solution. The main product was identified as C-S-H, and, in the pastes with high pH, hydrotalcite was observed at later stages of hydration. The pH of the mixing solution should be higher than pH 11.5 to effectively activate the hydration of GGBFS. As deduced from very low electrical conductivity measurements, GGBFS pastes had very tortuous and disconnected pores. The effect of the pH of the aqueous solution on the composition, microstructure and properties of alkali-activated GGBFS pastes are also discussed.

1. Introduction

Although slag without an activator does react with water, the rate of hydration is very slow. Ground Granulated Blast-Furnace Slag (GGBFS) is a glassy granular material formed when molten blast-furnace slag is rapidly cooled, usually by immersion in water, and then ground to improve its reactivity. The major components of blast-furnace slag are SiO_2, CaO, MgO, and Al_2O_3, which are common components in commercial silicate glasses. Its hydraulic reactivity depends on chemical composition, glass phase content, particle size distribution and surface morphology [1–3]. Blast-furnace slag has been used as a pozzolanic admixture in Portland cement paste [1–6].

Research on alkali activated slag (AAS) [6–17] has provided basic information about the mechanism of alkali-activation. Mehta [3] reported that coatings of aluminosilicate form on the surface of slag grains within a few minutes of exposure to water, and these coatings were impermeable to water. Unless a chemical activator is present, further hydration is inhibited. Portland cement, gypsum and many alkalies have been used as activators, and it has been observed that the rate of hydration is faster at high alkali concentrations. Compared to Portland cement-activated slag, alkali activated slag (AAS) has some advantageous properties including rapid development of high strength, good durability and high resistance to chemical attack [7, 16, 17].

The mechanical and rheological properties of slag pastes depend on the alkali activators used [8–12]. Goto *et al.* [13] found the solubility of synthetic silica-alumina gel is strongly affected by its composition and the pH of the solution. The main hydration product of GGBFS is calcium silicate hydrate (C-S-H) with a low Ca/Si ratio regardless of the activator used [6, 7, 10, 14, 15], but the morphology and composition of the hydration products change with the activator and other hydration conditions [14, 15]. Various studies of cementitious materials [18–30] suggest that the pH of the solution plays an important role in the hydration process and also in determining the nature of C-S-H formation. It has been reported that C-S-H doesn't form in a solution with a pH below 9.5 [18]. Also the formation of C-S-H is dependent on the types of silicate species in solution, which is also affected by pH [19, 20]. High [Si] in the aqueous solution comes with a low [Ca], and it has been shown that a high pH of the solution produces high [Si] [31]. The effect of pH on the structure and composition of C-S-H, however, is still controversial. While Andersson *et al.* [32] claimed there is no obvious correlation of pH with the chemical compositions of the solids, others reported that the C/S ratio of C-S-H depends on the pH and alkali content of the pore solution; C-S-H with high C/S ratio forms in solutions of high pH or high alkali content [21–26]. However, others have reported that C-S-H with a low C/S ratio forms in solutions of high pH or high alkali content [27–30, 33–35]. Unfortunately the lack of detailed knowledge on AAS hydration limits its wider use. The effect of alkali solutions of different pH on the hydration of GGBFS is reported here.

2. Experimental

The chemical composition of the GGBFS was 37.98% SiO_2, 7.93% Al_2O_3, 39.11% CaO, 11.45% MgO, 0.44% Fe_2O_3, 0.46% TiO_2, 0.31% Na_2O, 0.36% K_2O, and 0.62% MnO. The Blaine fineness was 5565 cm^2/g. It was mixed with DI water and NaOH solutions of 1M and 0.1M concentrations using a Hobart mixer for 5 min at speed setting 1. The mass ratio of solution to slag was 0.45 by weight. The mixes were cast into

plastic tubes and sealed before placing the samples in a 25 °C water bath.

The heat of hydration of the fresh pastes at 25 °C was measured using isothermal calorimetry, and the electrical conductances of the pastes and the pore fluids were measured using impedance spectroscopy (IS). The measurement of the electrical properties and the extraction of pore fluids have been described by Christensen [36] and Christensen *et al.* [37]. All the samples were sealed to minimize any carbonation or oxidation of samples. All filtration procedures were performed in a glove box under a nitrogen atmosphere, and samples were stored in a nitrogen-filled container. After the pastes became rigid, pore fluid was extracted using a high pressure steel die at the required ages; details are given elsewhere [38]. In another study [39] X-rays were used to identify crystal phases.

At specified times, samples of 2–3 mm thickness were sliced from cylinders of hardened cement paste for solvent exchange experiments. The samples were wiped with a wet lint-free tissue to remove excess surface moisture to measure the saturated surface dry (SSD) weight, and then immersed in methanol. Samples were periodically removed and weighed to obtain weight loss which correlates with the replacement of solvent and pore solution. When a constant weight was reached, large porosity (ϕ_{MeOH}), defined as the amount of methanol-accessible pores, was calculated using the following equation:

$$\phi_{\mathrm{MeOH}} = \frac{V_{\mathrm{cap}}}{V_{\mathrm{total}}} = \frac{\rho_{\mathrm{MeOH}}}{\rho_{\mathrm{water}} - \rho_{\mathrm{MeOH}}} \cdot \frac{(W_0 - W_{\mathrm{f}})}{(W_{\mathrm{SSD}} - W_0)} \quad (1)$$

where ρ_{MeOH} and ρ_{water} are the density of methanol and water respectively, W_0 is the weight of samples measured in methanol before the capillary pore solution is exchanged, W_{f} is the average constant weight after pore solution has been exchanged and W_{SSD} is the saturated surface dry weight. Methanol was used since it yielded an apparently conventional weight loss profile while that of isopropanol was anomalous [40, 41].

3. Results and discussion

3.1. Calorimetry

The heat evolution of GGBFS pastes mixed with 0.1M and 1M NaOH solutions are compared with that of GGBFS mixed with DI water in Fig. 1a. GGBFS pastes mixed with NaOH solution show an earlier and higher heat evolution peak than the paste mixed with DI water. The difference in peak height for the paste mixed with 0.1M NaOH solution and the paste with DI water is about 10% of the difference in height between the paste mixed with 1M NaOH solution and the paste with DI water. Thus the peak height appears to be directly proportional to the NaOH concentration. The heat evolution is defined using 2 parameters: dq/dt_{max}, which is the maximum height of the heat evolution curve, and t_{max}, the time at which dq/dt_{max} occurs. Both values depend on the concentration of NaOH as seen in Fig. 1b. When normalized by the values for DI water GGBFS paste, dq/dt_{max} linearly increases and t_{max} inversely decreases with the concentration of NaOH. These thermal characteristics can be used to predict the setting time and heat release of activated GGBFS paste.

3.2. Porosity

As measured by the amount of methanol-accessible pores, ϕ_{MeOH} of GGBFS pastes changed with time as shown in Fig. 2. The concentration of NaOH in the mixing solution is inversely related to ϕ_{MeOH}. It should be noted that GGBFS pastes have significantly larger volumes of porosity in comparison to OPC pastes [36, 37] when one assumes that only capillary pores are methanol-accessible. The volume of pores before reaction is 55.7% of the total volume of the paste, calculated from the density of GGBFS (2.79 g/cm^3). The measured amount of pores after 3 days of hydration was about the same for every paste. It is possible that some portion of gel water was exchanged with methanol, in addition to capillary water, since methanol is very small. Therefore the values in Fig. 2 should be considered as relative measures between different pastes, not the absolute amount of capillary pores.

The GGBFS paste mixed with 0.1M NaOH solution had values for volume of porosity very close to those of DI water mixed samples, while the samples activated by 0.5 and 1.0M NaOH solution were similar. The difference in ϕ_{MeOH} results from either the different degree of hydration or the formation of different microstructural features in GGBFS pastes of various concentration of NaOH. As discussed later, hydrotalcite was observed in higher pH pastes along with C-S-H. A more sophisticated study is required to determine its effect on various properties of GGBFS pastes.

3.3. Impedance spectroscopy (IS)

Impedance spectroscopy was used to obtain an accurate value of the electrical conductivity of the paste and the aqueous phase, σ and σ_0, respectively, which are shown in Fig. 3a and b. The normalized conductivity, σ/σ_0, is shown in Fig. 3c. The conductivities of the pastes were constant at early stages, and then decreased as hydration proceeded. The conductivities of the pore solutions were also affected by the pH of the initial mixing solution. The higher alkali concentration produced higher conductivities of pore fluids. During the 56 days of hydration, the conductivities of the pore fluids remained constant in the pastes mixed with NaOH solutions and changed only slightly at the later stages of hydration. However, the pastes mixed with DI water had pore fluids with continuously increasing conductivities. The alkali activator seems to control the conductivity of pore fluids at the early stage of hydration. The electrical conductivities of aqueous phases could be correlated with the concentration of Na ions in the aqueous phase of each paste. The concentration of Na ions in the aqueous phase was constant through 56 days of hydration in the pastes mixed with NaOH solutions, but it increased from 6.9 to 49.3 mmol in the paste mixed with DI water.

The electrical properties can be used to study the evolving pore structure [36, 37]. Various microstructural

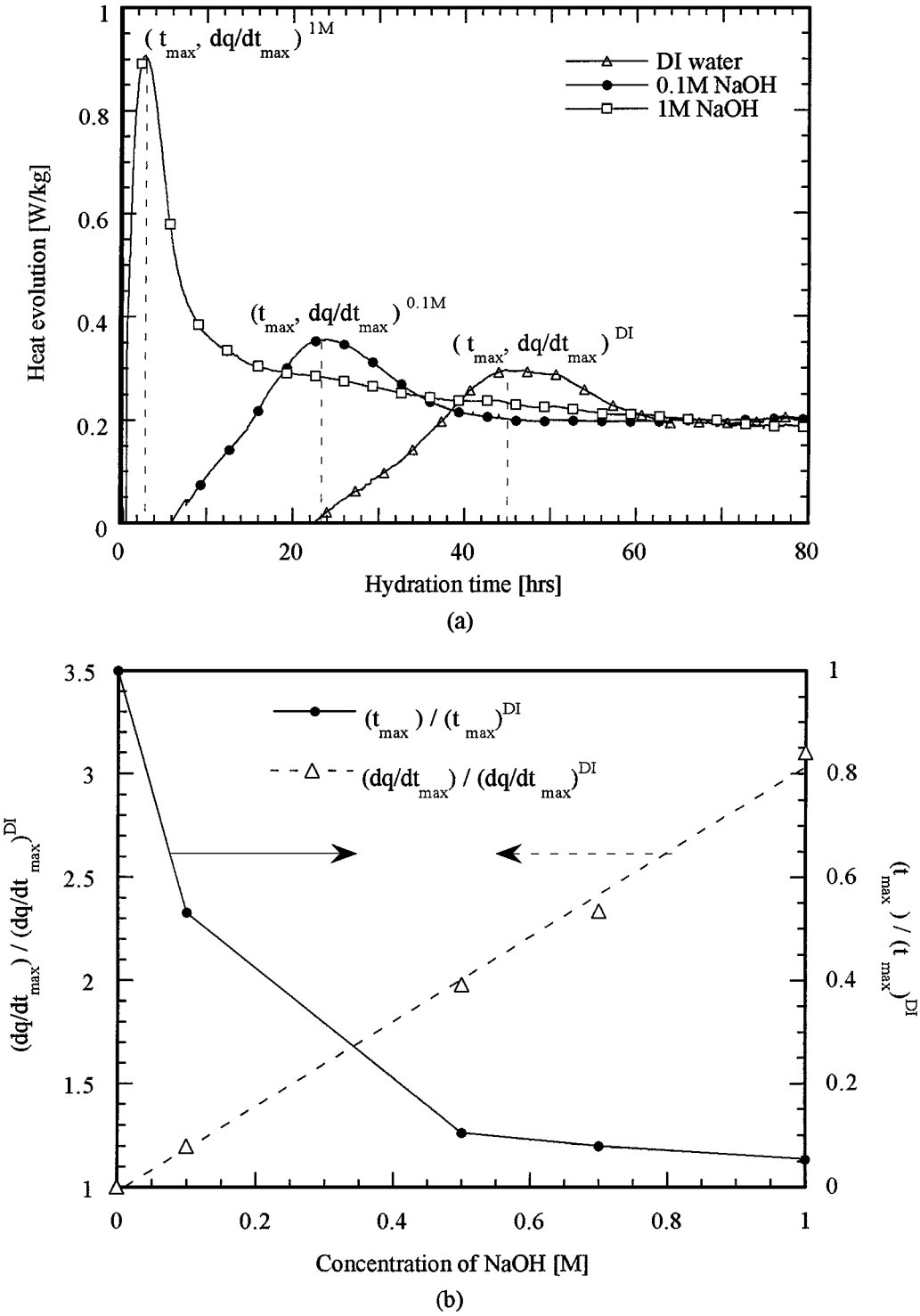

Figure 1 Heat of hydration of GGBFS pastes at 25 °C (a) the heat evolution measured by isothermal calorimeter and (b) dq/dt_{max} and t_{max} as a function of the concentration of NaOH.

factors are incorporated into the relationship [42]:

$$\sigma = \sigma_0 \phi_{cap} \beta \quad (2)$$

where σ is the overall conductivity of paste, σ_0 is the conductivity of the aqueous phase, ϕ_{cap} is the volume fraction of capillary porosity, and β is a connectivity (inverse tortuosity) factor. Since both ϕ_{cap} and β decrease with hydration time, σ/σ_0, the normalized conductivity of paste also decreases.

The pore structure factor, β, is calculated using Equation 2 and the values of porosity from Fig. 2. These are shown as a function of hydration time in Fig. 4a and as a function of porosity in Fig. 4b. The decrease of β with hydration is indicative of both the filling of pores and the decreasing connectivity of the pore structure. The β values for GGBFS pastes are more than an order of magnitude smaller than they are in conventional cements [36, 37], and it is apparent that GGBFS pastes have a very disconnected pore structure. It should be noted that the volume of the pore depends on the methods by which it is measured. For example, methanol exchange appears to include some gel pores

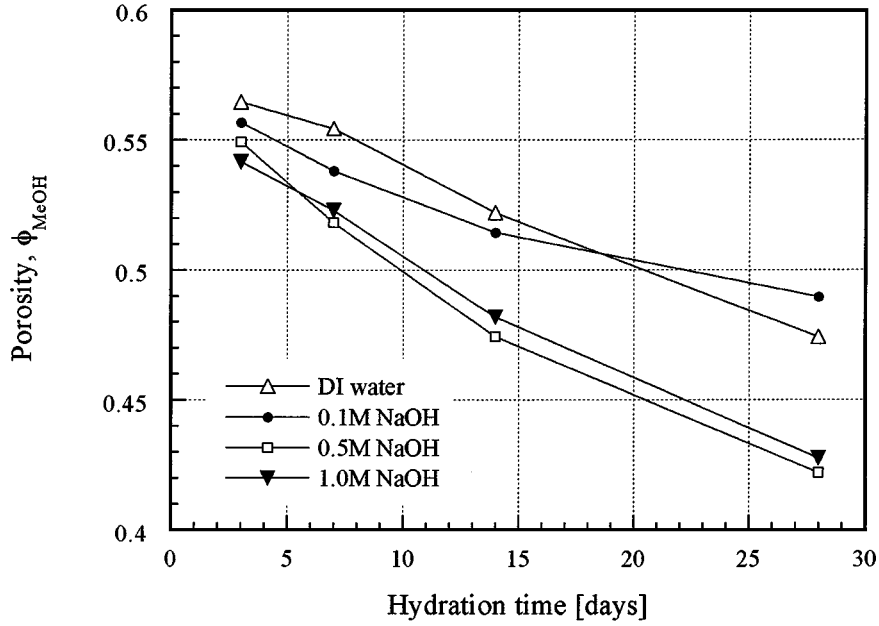

Figure 2 The volume fraction of pores, ϕ_{MeOH}, for GGBFS pastes measured by solvent exchange using methanol.

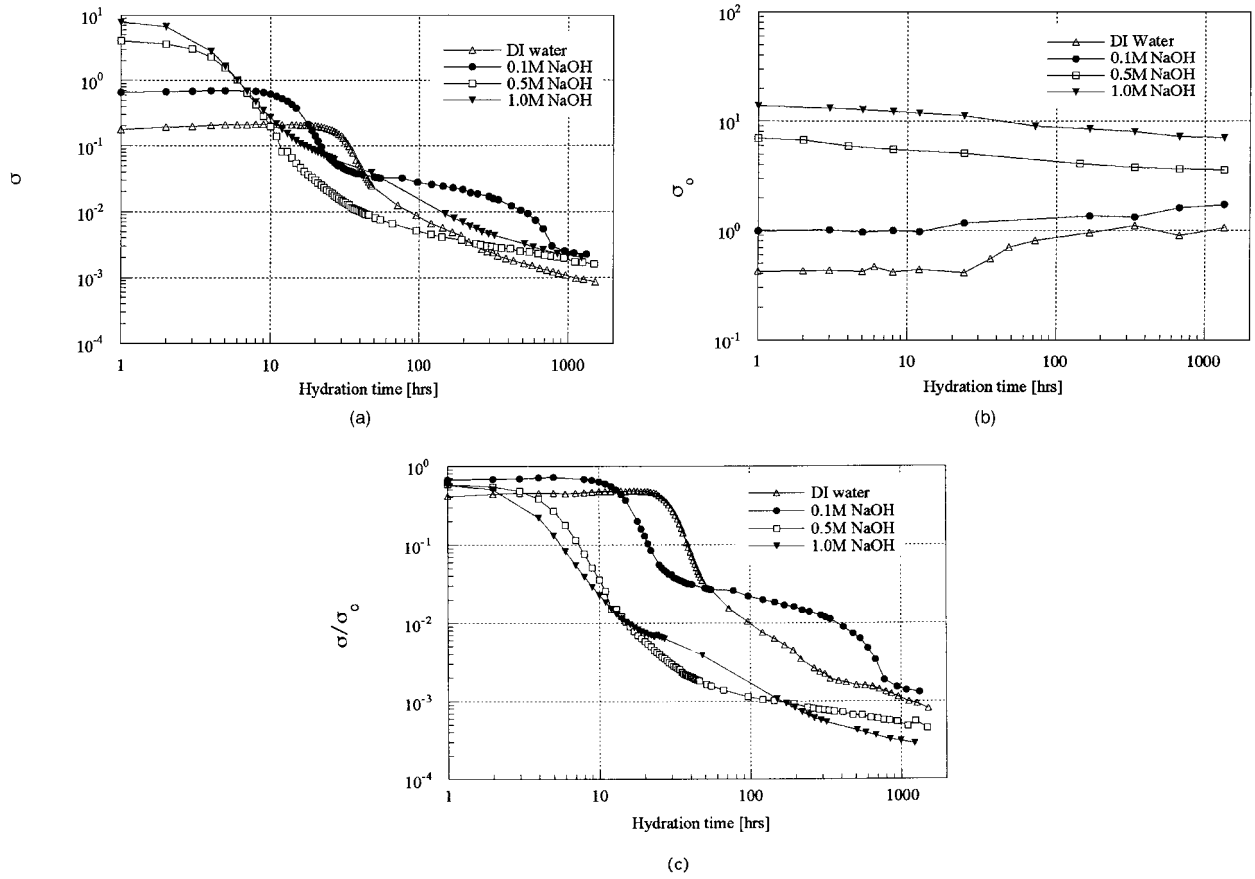

Figure 3 The electrical conductivity of (a) bulk, σ, and (b) pore solution, σ_0, and (c) normalized conductivity, σ/σ_0, of GGBFS pastes measured using impedance spectroscopy.

as well as capillary pores. It is very important to have accurate values for capillary pores as they contribute to electrical conduction if exact values of β are to be determined. However, compared to OPC, white portland cement (WPC), and C_3S pastes [37], values of σ/σ_0 for GGBFS paste are one or two orders magnitude smaller, and values for GGBFS pastes activated by NaOH are even less. At 28 days, the σ/σ_0 of GGBFS pastes mixed with NaOH solutions is about one order of magnitude smaller than that of the pastes mixed with DI water.

3.4. Environmental secondary electron microscopy (ESEM)

The microstructure of each sample was observed using ESEM at 7 days of hydration and compared to one another as shown in Fig. 5. GGBFS pastes showed

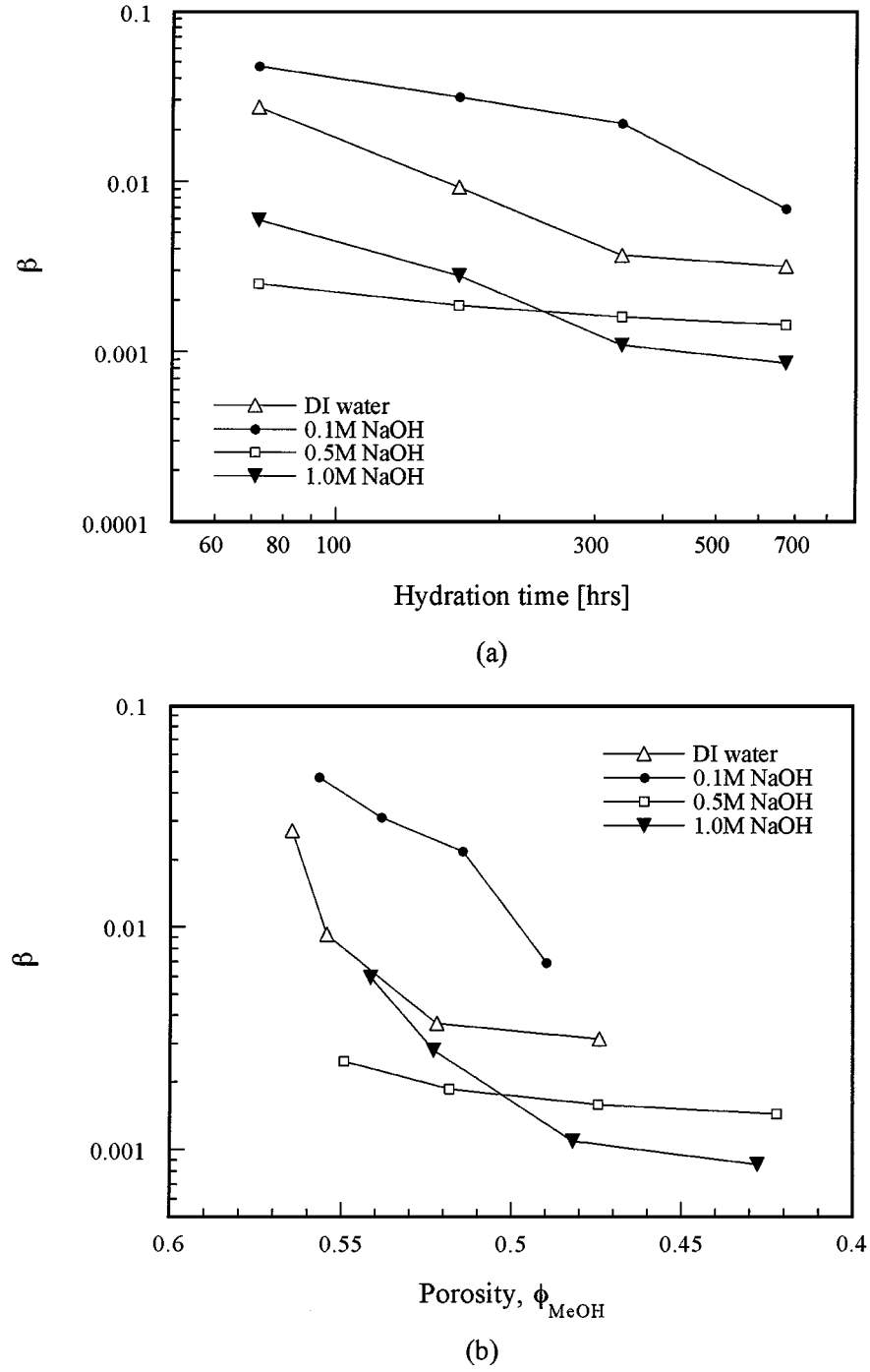

Figure 4 Pore structructure factor, β as a function of hydration time and (b) porosity, ϕ_{MeOH}, for GGBFS pastes.

very smooth, homogeneous and interconnected-solid in all samples. Pores between grains look very tortuous, and some of them appear isolated from others. The similarity of microstructure in GGBFS pastes regardless of the concentration of NaOH is because C-S-H is the main hydration product in every sample, and the relatively small amount of hydrotalcite (as detected by X-rays [39]) isn't easily distinguished from C-S-H. Higher concentrations of NaOH, however, gave higher degrees of reaction and more filled pores, hence, a less porous microstructure.

3.5. Pore solution analysis

Analysis of pore solutions has been reported in ref 39. Also, based on equilibrium constants, activities of Si and Ca have been computed as a function of pH. This relationship between pH and ionic concentration was explained using the equilibrium solubility product, which depends on the Gibbs free energy of dissolution. For example, the solubility of Si in aqueous solution is controlled by the standard free energy, ΔG^0, and the thermodynamic equilibrium constant, K, of different silicate ions as given in Table I. The reactions described in Table I are also shown as broken lines in Fig. 6a and b. Assuming the activity of $SiO_{2\,(quartz)}$ is 1, the activity of H_2SiO_3 in aqueous solution, $\alpha_{(H_2SiO_3)}$ becomes constant, and the activity of $HSiO_3^-$ ion, $\alpha_{(HSiO_3)}$, is determined by pH and $\alpha_{(H_2SiO_3)}$. Using the standard free energy, $\Delta G^0 = -RT \ln K$, $\alpha_{(HSiO_3)}$ becomes equivalent to $\alpha_{(H_2SiO_3)}$ at pH 10 and then linearly increases with pH.

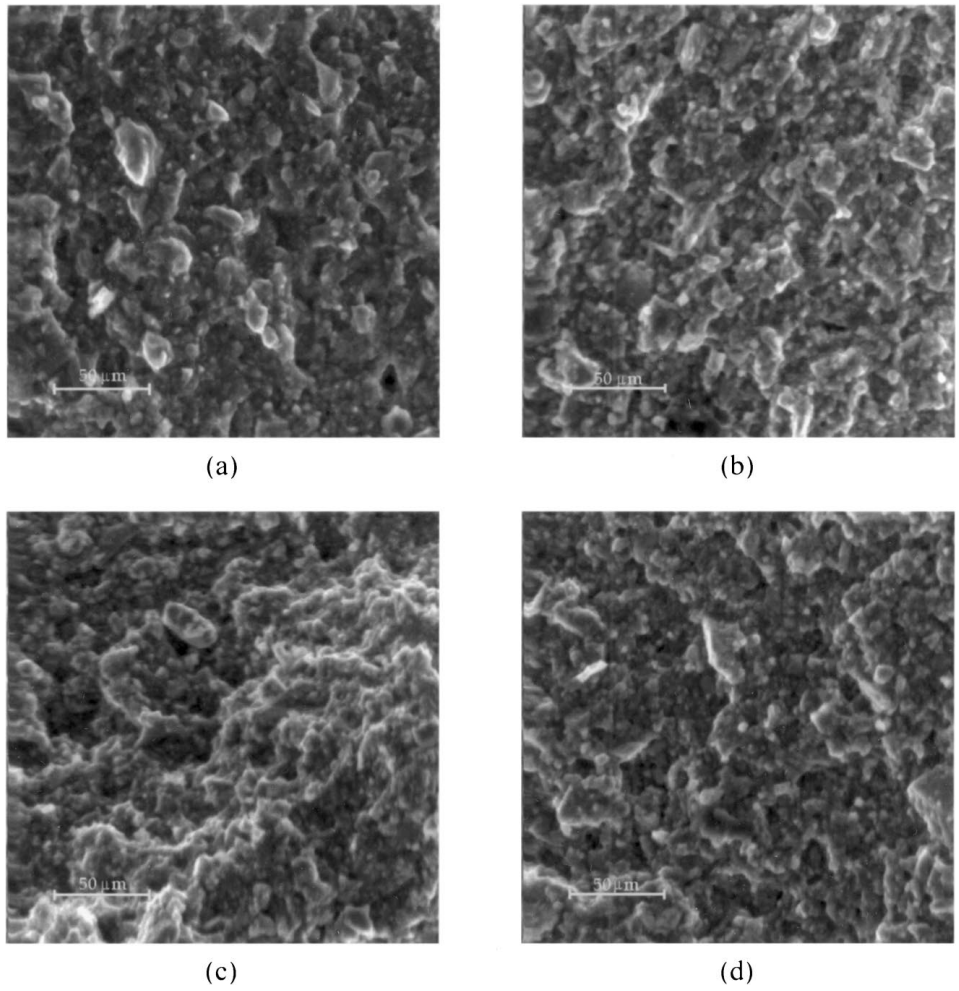

Figure 5 ESEM micrographs of GGBFS pastes mixed with (a) DI water, (b) 0.1M, (c) 0.5M and (d) 1.0M NaOH solutions at 7 days of hydration.

Thus even vitreous silica becomes unstable at pH 10. When the same calculation is repeated for Ca, the concentration of Ca in aqueous solution is dominated by $Ca(OH)_2$ levels below pH 11.5, and by Ca^{2+} above pH 11.5. The low concentration of Ca in highly alkaline solution is due to the low solubility of $Ca(OH)_2$ above pH 11.5. This thermodynamic prediction has been verified for alkaline-lime-silicate glasses [34, 35].

However, all the calculations above use the standard thermodynamic data taken at 25 °C for crystalline phases. GGBFS is not a crystalline material, and therefore has a different standard free energy of formation from pure silica or quartz. The Gibbs free energy of formation for an amorphous phase is usually higher than that for a crystalline phase, and this difference affects both solid and aqueous phases. Although this changes the absolute magnitude of the activities, it does not change the trend with respect to pH. As reported in Song and Jennings [39], the aqueous concentrations of Si and Ca in pore fluids show the same trend as thermodynamic activity. In our study, the concentration of Si started to increase around pH = 11.5, while the values from thermodynamic calculations show pH = 10 as the activity of silicate ions in the aqueous phase increases. The decrease in the solubility of Ca with pH can be explained similarly considering the reactions involving Ca ions as shown in Table I. At pH > 11.5, the Ca ion concentration in the aqueous solution drops since the solid phase is thermodynamically favored; that is, the low concentration of Ca in this region is due to the lower equilibrium aqueous solubility of $Ca(OH)_2$ in highly alkaline solution. The pH-dependent solubility of Si seems to be the most important factor explaining the alkali-activation of GGBFS thermodynamically. With

TABLE I Standard free energy and thermodynamic equilibrium constants of different ions in aqueous solution at 25 °C [35]

Reaction	ΔG^0 (kcal/mol)	log K[a]
$SiO_{2\,(quartz)} + H_2O = H_2SiO_{3\,(aq)}$	7.1	$-5.20 = \log \alpha\ (H_2SiO_3)$
$H_2SiO_{3\,(aq)} = HSiO^-_{3\,(aq)} + H^+$	13.6	$-15.2 = \log \alpha\ (HSiO_3^-) - \text{pH}$
$H_2SiO_{3\,(aq)} = SiO^{2-}_{3\,(aq)} + 2H^+$	30.0	$-27.2 = \log \alpha\ (SiO_3^{2-}) - 2\ \text{pH}$
$CaO + H_2O = Ca(OH)_{2\,(aq)}$	−6.28	$4.6 = \log \alpha\ (Ca(OH)_2)$
$Ca(OH)_{2\,(aq)} + 2H^+ = Ca^{2+}_{(aq)} + 2H_2O$	−31.3	$27.6 = \log \alpha\ (Ca^{2+}) + 2\ \text{pH}$

[a] $\ln K = -\Delta G^\circ / RT = 2.303 \log K$

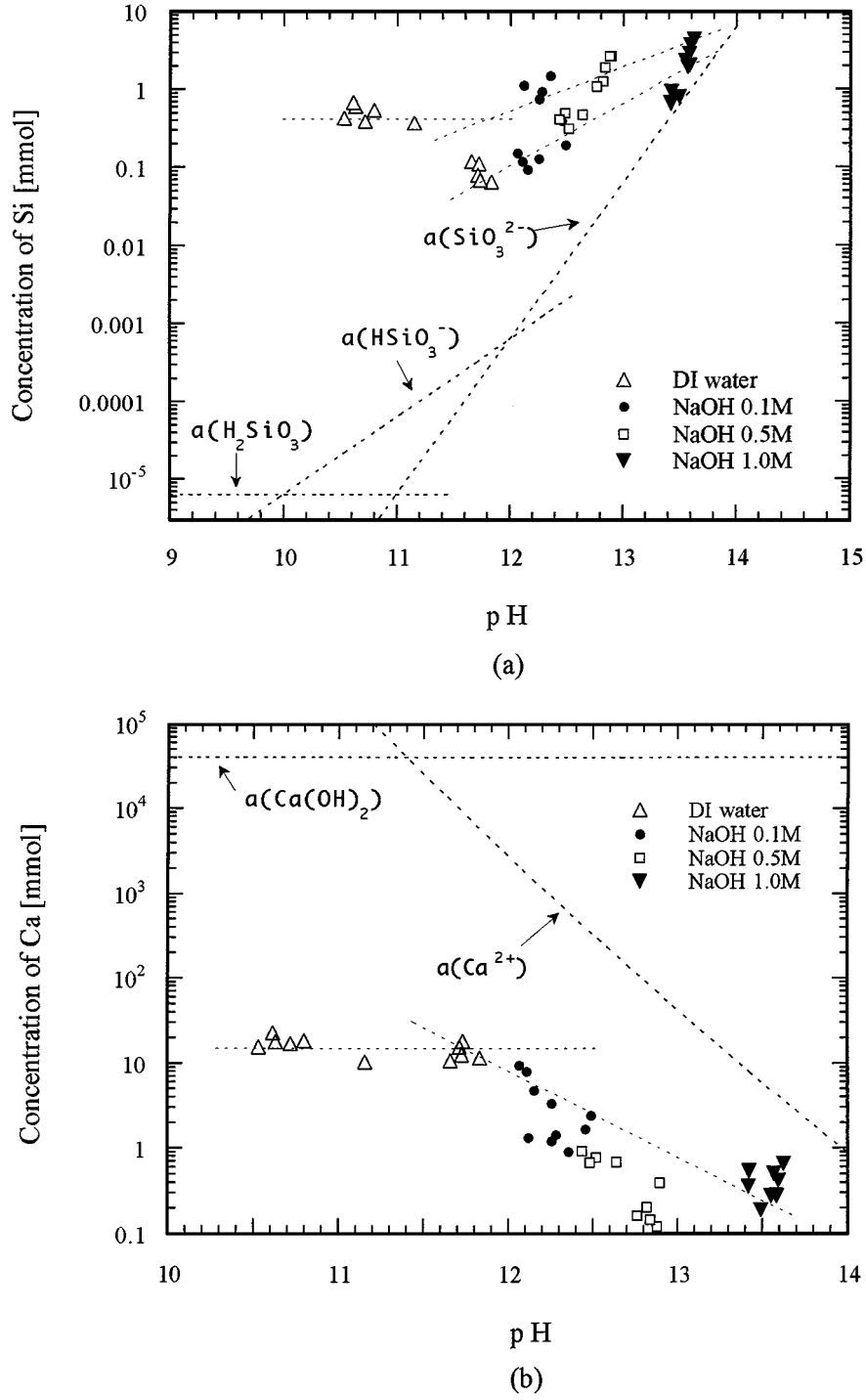

Figure 6 The concentration of (a) Si and (b) Ca as a function of pH of pore fluids. (The activities of ions in aqueous phase calculated in ref 39 are also plotted in the same scale as dotted lines.)

a solution pH below 11.5, it is hard to solubilize silica in spite of the presence of a chemical activator in the aqueous phase.

In Fig. 6a, the data suggest the existence of two separate lines above pH 11.5. Considering the age of the pastes and the results from calorimetry, IS, and XRD, the line with a higher Si concentration might be associated with the fresh pastes before or during the very early stage of C-S-H formation. The data on the line with a lower Si concentration are from a later stage of hydration. After C-S-H forms in the paste, the thermodynamic equilibrium described in Table I must be changed to include the new solid phase, C-S-H, and the solubility of Si should be determined by C-S-H, pH and the solubility of Ca in pore fluid.

In Fig. 7, the Si concentration is plotted against the Ca concentration and superimposed on the water rich region of the CaO-SiO_2-H_2O phase diagram [43, 44] containing the solubility of two types of C-S-H. In this study, the equilibrium state of C-S-H in the GGBFS pastes apparently depends on pH. The reaction mechanism may be the same, but the solubility of Ca and Si changes with pH and leads to the formation of different hydration products. The C-S-H formed in NaOH solutions causes the solubility of Ca and Si to reside on Curve S, but C-S-H formed in DI water is in equilibrium

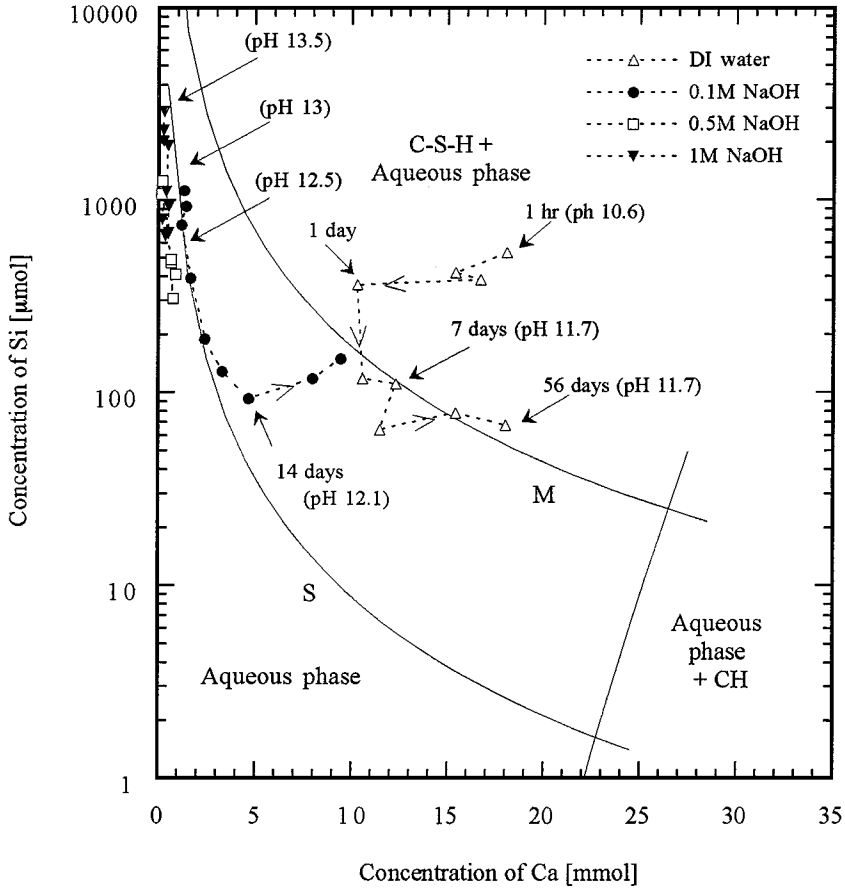

Figure 7 Concentration of Si and Ca on the water-rich region of the CaO-SiO_2-H_2O phase diagram. The arrow heads indicate the direction of time.

with the aqueous phase on Curve M. The C-S-H that is formed in the paste and mixed with 0.1M NaOH shows solubility of Ca and Si very close to Curve M after 28 and 56 days of hydration. Considering the pH of the pastes mixed with DI water and the paste with 0.1M NaOH after 14 days of hydration, it may suggest the pH of pore fluids is a very important variable in controlling the ionic solubilities and the equilibrium state of C-S-H. Compared to the Ca/Si ratio of the C-S-H that was determined by thermodynamic analysis [44], the Ca/Si ratio was lower than 1 in the GGBFS pastes mixed with 1M NaOH solution (pH 13.5) and about 1 in the paste mixed with 0.1M NaOH solution (pH 12.5) at 28 days. Since the solubility of Si increases with pH while that of Ca decreases, pastes with a higher pH pore solution must have C-S-H with a lower Ca/Si ratio.

It has been suggested that a high pH solution activates the hydration of slag by solubilizing the water-impermeable layer on the surface of slag particles [3, 7]. This study suggests that the pH of the mixing solution may also affect the nature of C-S-H and its Ca/Si ratio by controlling the solubility of each component. As seen in Fig. 7, the low concentration of Ca and high concentration of Si are thermodynamically favored at a higher pH, and it allows the formation of hydration products of low Ca/Si ratio. The microstructure of GGBFS pastes may vary according to the pH of the pore solution and the Ca/Si ratio of the C-S-H. Several studies [4, 5, 15] have shown that increasing slag content in OPC pastes reduces the Ca/Si ratio of C-S-H and progressively changes the morphology of the hydration products. The more slag that exists in OPC paste, the lower the Ca/Si ratio of C-S-H. Also, the C-S-H of low Ca/Si has a foil-like morphology compared to the fiber-like C-S-H of a high Ca/Si ratio. Richardson *et al.* [45] also pointed out that GGBFS pastes showed a foil-like morphology whether they were mixed with 5M KOH or just water. C-S-H with different Ca/Si ratios show different morphologies, hence, the microstructure of hydrated slag pastes and other properties, like permeability and mechanical strength, are expected to change. The relationship between the morphology of C-S-H and the macroscopic properties of pastes needs more investigation.

4. Summary and Conclusions

Taken together, the results reported in this paper may suggest that C-S-H with a solubility on Line S, Fig. 7, has a microstructure different from that with solubility on Line M. The reaction rate is faster and the structure factor, β, is lower for C-S-H that forms in contact with aqueous phase on Line S than for C-S-H in contact with aqueous phase on Line M. According to Fig. 4, the 0.1M NaOH sample starts on Line M and transfers to Line S, suggesting that this trend is true even for one sample. Somehow the C-S-H is allowed to form in the entrances to pores if the aqueous phase is on line S, and this may be the result of greater diffusion distances before reaction at lower Ca concentrations. The addition of NaOH as an activator buffers the pH of pore fluids. The rate of hydration depends on the pH of the solutions: the higher the concentration of NaOH, the faster the hydration of GGBFS. A linear relationship

was found between dq/dt_{max} and NaOH concentration, and an inverse relationship was found between t_{max} and the NaOH concentration. NaOH-activated GGBFS pastes have more capillary porosity compared to conventional cement pastes. The concentration of NaOH in the initial mixing solution significantly affected the formation of the main hydration product, C-S-H. Very low values of paste conductivity were observed in GGBFS pastes. Low σ/σ_0 results from the very low connectivity and high tortuosity of the pore structure. Regardless of the concentration of NaOH, GGBFS pastes show very similar microstructure. Less porosity in samples with higher pH is attributed to a higher degree of hydration.

References

1. ACI Committee 226, *ACI Manual of Concrete Practice*, 226.1R. (1989) pp. 1–16.
2. H. UCHIGAWA, in Proceedings of the 8th International Congress on the Chemistry of Cement, Rio de Janeiro, 1986, Vol. 3, p. 249.
3. P. K. MEHTA, in Proceedings of the 3rd International Conference on Fly Ash, Silica Fume, and Natural Pozzolans in Concrete, Tronheim, Norway, 1989, pp. 1–43.
4. T. HAKKINEN, *Cem. Concr. Res.* **23** (1993) 407.
5. *Idem., ibid.* **23** (1993) p. 518.
6. M. REGOURD, J. H. THOMASSIN, P. BALLIF, and J. C. TOURAY, *ibid.* **13** (1983) 549–556.
7. B. TALLING and J. BRANDSTETR, in Proceedings of the 3rd International Conference on Fly Ash, Silica Fume, and Natural Pozzolans in Concrete, Tronheim, Norway, 1989, p. 1519.
8. C. QING-HUA and S. L. SARKAR, *Advanced. Cem. Bas. Mat.* **1** (1994) 178.
9. S. D. WANG, K. L. SCRIVENER and P. L. PRATT, *Cem. Concr. Res.* **24** (1994) 1033.
10. W. J. CLARKE and M. HELAL, in Proceedings of the 1st International Conference on Alkaline Cements and Concretes, edited by P. V. Krivenko, Kiev, Ukraine, October 1994, p. 151.
11. W. J. CLARKE and M. D. BOYD, in Proceedings of ACI International Conference, Singapore, 1994, edited by V. M. Malhotra (1994) p. 141.
12. Z. HUANHAI, W. XUEQUAN, X. ZHONGZI and T. MINGHU, *Cem. Concr. Res.* **23** (1993) 1253.
13. S. GOTO, K. AKAZAWA and M. DAIMON, *ibid.* **22** (1992) 1216.
14. S. D. WANG and K. SCRIVENER, *ibid.* **25** (1995) 561.
15. I. G. RICHARDSON and G. W. GROVES, *J. Mater. Sci.* **27** (1992) 6204.
16. S. D. WANG, *Mag. Concr. Res.* **43** (1991) 29.
17. V. D. GLUKHOVSKY, G. S. ROSTOVSKAYA and G. V. RUMYAY, in Proceedings of 7th International Congress on the Chemistry of Cement, Paris, 1986, Vol. III, V164–V168.
18. S. A. GREENBERG and T. N. CHANG, *J. Phys. Chem.* **69** (1965) 182.
19. H. M. JENNINGS, "The Developing Microstructure in Portland Cement" in "Advances in Cement Technology," edited by S. N. Ghosh (Pergamon Press, New York, 1983).
20. H. F. W. TAYLOR *et al., Mater. Const. (Paris)* **17** (1984) 457–468.
21. E. P. FLINT and L. A. WELLS, *J. Res. Nat'l, Bur. Stand. (US)* **12** (1934) 751.
22. P. S. ROLLER and G. ERVIN, JR., *J. Amer. Chem. Soc.* **62** (1940) 461.
23. S. A. GREENBERG, T. N. CHANG and E. ANDERSON, (1960) 1151.
24. K. G. MCCURDY and H. N. STEIN, *Cem. Concr. Res.* **3** (1973) 247.
25. *Idem., ibid.* **3** (1973) 509.
26. A. R. RAMACHANDRAN and M. W. GRUTZECK, *J. Amer. Ceram. Soc.* **76** (1993) 72.
27. G. L. KALOUSEK, *J. Res. Nat'l, Bur. Stand. (US)* **32** (1944) 285.
28. K. SUZUKI, T. NISHIKAWA, H. IKENAGA and S. ITO, *Cem. Concr. Res.* **16** (1986) 333.
29. K. SUZUKI, T. NISHIKAWA and S. ITO, *Cem. Concr. Res.* **15** (1985) 213.
30. D. MACPHEE, K. LUCK, F. P. GLASSER and E. E. LACHOWSKI, *J. Amer. Ceram. Soc.* **72** (1989) 646.
31. S. A. GREENBERG and E. W. PRICE, *J. Phys. Chem.* **61** (1957) 1539.
32. K. ANDERSSON *et al., Cem. Concr. Res.* **19** (1989) 327.
33. H. F. W. TAYLOR, "Cement Chemistry" (Academic press, London, 1990) p. 282.
34. T. M. EL-SHAMY, J. LEWINS and R. W. DOUGLAS, *Glass Technol.* **13** (1972) 81.
35. A. PAUL, "Chemistry of Glasses" (Chapman and Hall, London and New York, 1982) p. 108.
36. B. J. CHRISTENSEN, "Microstructure Studies of Hydrating Portland Cement-Based Materials Using Impedance Spectroscopy," PhD thesis, Northwestern University, 1993, pp. 103–115.
37. B. J. CHRISTENSEN, R. T. COVERDALE, R. A. OLSON, S. J. FORD, E. J. GARBOCZI, H. M. JENNINGS and T. O. MASON, *J. Amer. Ceram. Soc.* **77** (1994) 2789.
38. R. S. BARNEYBACK and S. DIAMOND, *Cem. Concr. Res.* **11** (1981) 279.
39. S. SONG and H. M. JENNINGS, *Cem. Concr. Res.* **29** (1999) 159.
40. D. C. HUGHES, *ibid.* **18** (1988) 321.
41. D. C. HUGHES and N. L. CROSSLEY, *ibid.* **24** (1994) 1255.
42. E. J. GARBOCZI, *ibid.* **19** (1989) 327.
43. H. M. JENNINGS, *J. Amer. Ceram. Soc.* **69** (1986) 614.
44. E. M. GARTNER and H. M. JENNINGS, *J. Amer. Ceram. Soc.* **70** (1987) 743.
45. I. G. RICHARDSON, A. R. BROUGH, G. W. GROVES and C. M. DOBSON, *Cem. Concr. Res.* **24** (1994) 819.

Received 19 May 1997
and accepted 10 March 1999